PAPER • **OPEN ACCESS**

Systematic investigation of stripline width and contact metal effects on terahertz photoconductive antenna performance

To cite this article: I Nevinskas *et al* 2026 *Phys. Scr.* **101** 105503

Physica Scripta

OPEN ACCESS

RECEIVED
10 October 2025

REVISED
13 January 2026

ACCEPTED FOR PUBLICATION
19 February 2026

PUBLISHED
9 March 2026

PAPER

Systematic investigation of stripline width and contact metal effects on terahertz photoconductive antenna performance

I Nevinskas[1,*], M Kamarauskas[1], V Kovalevskij[1], D Vizbaras[2], K Ikamas[1,2], M E Daraei[1], A Bičiūnas[1] and V Pačebutas[1]

[1] Center for Physical Sciences and Technology, Saulėtekio al. 3, Vilnius, 10257, Lithuania
[2] Institute of Applied Electrodynamics and Telecommunications, Vilnius University, Saulėtekio al. 3, Vilnius, 10257, Lithuania
[*] Author to whom any correspondence should be addressed.

E-mail: ignas.nevinskas@ftmc.lt

Keywords: photoconductive antenna, terahertz time-domain spectroscopy, THz-TDS, coplanar stripline, contact metallization, AuGe/Ni/Au, titanium

Abstract

We systematically investigated terahertz photoconductive antennas on GaAs incorporating coplanar striplines of varying widths and two types of contact metallizations (AuGe/Ni/Au and standalone Ti). Measurements of the emitted terahertz power show that AuGe contacts yield stronger emission under low-bias conditions, whereas Ti contacts - initially constrained by Schottky barriers - exhibit superior performance at high bias due to barrier lowering. Terahertz time-domain spectroscopy further confirms the expected classical antenna behavior: decreasing the stripline width shifts the resonance frequency to higher values. At the shortest dipole lengths, however, the emitted spectra of the two metallizations diverge, with Ti-metalized antennas exhibiting higher resonance frequencies. These findings demonstrate that the performance of terahertz photoconductive antennas is constrained by the impedance of metallic contacts, providing essential design considerations for next-generation devices intended to operate at higher terahertz frequencies.

1. Introduction

Photoconductive antennas (PCAs) are widely used as compact and efficient room-temperature sources and detectors of terahertz (THz) radiation [1–3]. Their operation relies on both the ultrafast semiconductor substrate and the electrode contacts. The electrodes provide the bias field for carrier acceleration while simultaneously functioning as antennas that determine gain, bandwidth, and stability. At THz frequencies, however, the impedance of metallic contacts becomes significantly frequency dependent, the skin effect confines current to tens of nanometers near the surface, the current acquires a phase lag, and the classical half-wave dipole approximation no longer accurately describes the radiation characteristics [4, 5]. As a result, the electrode geometry and material composition strongly affect impedance matching with the photocarriers.

Electrode geometry and configuration [5–9] strongly influence the electric field distribution within the photoconductive gap, thereby governing both the efficiency and the spectral content of the generated THz pulses. Systematic studies of H-shaped electrode designs have examined how detection depends on gap width [10] and how emission scales with electrode length and width [11]. A consistent trend predicted by classical antenna theory has emerged: reducing the dipole length shifts the spectral peak to higher frequencies. Despite these insights, the simplest geometry - the coplanar stripline - remains comparatively underexplored. Previous studies have shown that the gap width influences the THz pulse amplitude [12], but the role of the stripline width, particularly its impact on the spectral maximum, has received little attention [13, 14]. This lack of systematic investigation leaves a critical gap in understanding the fundamental spectral limitations of PCAs.

In this work, we present a systematic experimental study of a coplanar stripline PCA, examining its performance as a function of stripline width - varied from 20 to 100 μm - and electrode metallization, comparing conventional AuGe/Ni/Au ohmic contacts [12, 14–17] with standalone Ti. Specifically, we investigate how

these parameters affect the emitted THz power under varying bias voltages, and we employ THz time-domain spectroscopy (THz-TDS) with matched emitter-detector pairs for each strip width to determine the spectral maximum and bandwidth. The results are interpreted within the framework of classical half-wave dipole theory, enabling us to identify the significance of electrode-related limitations to antenna performance. By addressing the largely overlooked influence of stripline width and metallization, this study aims to identify routes for shifting the emission maximum to higher frequencies and extending PCA operation across the full THz range (0.1–10 THz), beyond the typical 5–7 THz cutoff observed in GaAs-based devices.

2. Fabrication and experimental details

To investigate the influence of stripline width and metallization on PCA performance, we fabricated a series of devices under controlled conditions. Metallic coplanar striplines, 5 mm in length and 20–100 μm in strip width, separated by a 50 μm photosensitive gap, were patterned on a semi-insulating GaAs using laser lithography. Two metallization schemes were implemented: AuGe/Ni/Au (140/25/40 nm) and 1 μm-thick standalone Ti, both deposited by electron-beam evaporation and defined by lift-off in acetone. The AuGe/Ni/Au devices were additionally annealed at 400 °C for 90 s to lower contact resistance [12, 15, 16]. The substrates were then ion-damaged to achieve a carrier lifetime of approximately one picosecond [18, 19], as measured using optical pump—THz probe technique. Finally, the fabricated antennas were cleaved into 7 × 2 mm chips and mounted on 12 mm-diameter hyperhemispherical high-resistivity silicon lenses, truncated at 8 mm to enhance THz outcoupling.

The emitted THz power was measured with a broadband pyroelectric detector, using a mechanical chopper at 10 Hz to modulate the excitation laser. Spectral measurements were performed in a conventional THz-TDS setup employing two off-axis parabolic mirrors, as illustrated in figure 1(a). To avoid uncertainties arising from differing emitter and detector responses, matched emitter-detector pairs were used for each strip width and metallization.

All experiments were performed using a femtosecond laser with a 780 nm wavelength, 80 MHz repetition rate, and 80 fs pulse duration. For THz power measurements, the antennas were illuminated with 50 mW of average optical power, focused to a 50 μm-diameter spot using a 5 cm focal-length lens (fluence: 31.8 $\mu J/cm^2$). For THz-TDS measurements, both the emitter and detector were illuminated with 25 mW (fluence: 15.9 $\mu J/cm^2$), while the emitter was biased at 100 V.

3. Results and discussion

Figure 2 summarizes the dependence of emitted THz power on bias voltage and strip width for PCAs with AuGe and Ti contacts. At low bias, AuGe devices emit more power than Ti devices, indicating that carrier injection at the AuGe interface is less restricted, enabling a stronger internal electric field in the photoconductive gap. This results in a stronger internal electric field and a larger, faster photocurrent surge following optical excitation. In contrast, Ti devices exhibit much weaker emission in this regime because the Schottky barrier at the Ti/semiconductor interface reduces the effective field in the gap and suppresses carrier transport. Once the bias exceeds approximately 20 V, however, Ti devices undergo a rapid increase in emitted power. At high fields (120 V and above), AuGe and Ti devices deliver comparable power, indicating that the Schottky barrier no longer limits photocurrent generation. This steep high-field growth in Ti devices is consistent with field-induced modification of the Schottky barrier - such as barrier lowering or enhanced tunneling - which would increase carrier injection and strengthen the transient photocurrent [20].

Figure 2(b) shows the influence of strip width at fixed bias voltages of 50, 100, and 150 V. For AuGe devices, the emitted power increases with width up to about 50–60 μm and then gradually decreases, indicating an optimum in this range. At 150 V, for example, the 50-μm AuGe device produces 33 % more power than the 20-μm device, increasing from 36 to 48 μW. This trend persists across all investigated bias voltages. In general, maximum power emission occurs when reflections between the source and load are minimized - that is, when their impedances are matched. Therefore, the observed maximum likely corresponds to the stripline width at which the antenna impedance (the load) most closely matches the photocarrier impedance (the source).

In contrast, Ti-based devices do not exhibit a clear optimum, likely because their resistivity - more than an order of magnitude higher - enhances susceptibility to local heating, which may obscure the emergence of a distinct maximum. In addition, the substantially different impedance suggests that any optimum would occur at carrier concentrations significantly different from those of AuGe devices. Nevertheless, a weak but overall increasing trend in emitted power with increasing strip width is observed.

The THz-TDS spectra in figure 3 reveal a clear dependence of emission on both strip width and metallization. All devices exhibit the characteristic low-frequency rise, a spectral maximum in the few-hundred-

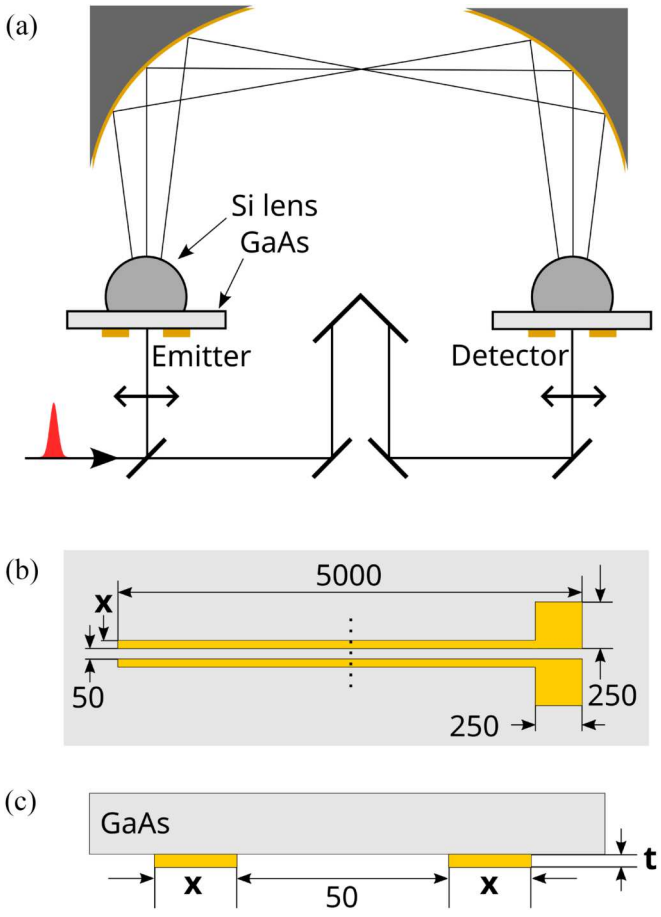

Figure 1. (a) Schematic of the THz-TDS setup used for PCA spectral characterization. (b) Schematic top view of a PCA, indicating the strip width parameter **x**. (c) Cross-sectional (profile) view of the PCA along the dashed line in (b), showing the metallization thickness **t**. Dimensions are in micrometers.

gigahertz range, and a subsequent roll-off at higher frequencies. Both the position of the spectral maximum and the extent of the high-frequency tail are strongly influenced by the electrode geometry. Narrow strips peak at higher frequencies and exhibit a broader bandwidth, whereas increasing the strip width (i.e., the effective dipole length) shifts the maximum toward lower frequencies and results in a more rapid spectral roll-off.

This spectral evolution can be understood by treating the PCA as a cascade of low-pass filters acting on the ultrafast photocurrent. The photocurrent is initiated by the femtosecond laser pulse, which by itself would support a broad Gaussian spectrum extending well beyond 5 THz for an 80 fs pump pulse ($f_{peak} = \frac{\sqrt{2\ln 2}}{\pi\,\Delta t}$). However, successive filtering stages within the device selectively suppress high-frequency components. The semiconductor response imposes limitations through the carrier lifetime (τ) and the momentum scattering time (τ_m). For example, a lifetime of $\tau = 1$ ps corresponds to a cutoff frequency near 0.16 THz, while a scattering time of $\tau_m = 108$ fs [21] corresponds to 1.5 THz. Carrier lifetime may therefore contribute to the suppression of high-frequency components, although it can be readily shortened by introducing additional ion-induced damage in the semiconductor. In contrast, the most challenging low-pass limitation to mitigate in practice arises from the characteristic energy-decay time τ_{ant}, which is set by the antenna geometry and contact material.

We compare the experimental results with a simple half-wave dipole model on a thick dielectric, $f_r = \frac{c}{2L\sqrt{\frac{1+\epsilon_d}{2}}}$, where c is the speed of light, ϵ_d is the GaAs permittivity, and L is the effective dipole length, approximated here as twice the strip width, corresponding to the limiting case of a vanishing gap. The extracted data from the spectra together with the model is presented in figure 4. The figure highlights how both strip width and metallization influence the peak frequency and the bandwidth, quantified by the full width at half maximum (FWHM). The converging experimental trends indicate that, for strip widths above approximately 120 μm, the model provides a reasonable estimate of the PCA response, consistent with a resonance-dominated regime.

At narrower strip widths, corresponding to peak frequencies above 220 GHz, increasing deviations from the model are apparent, with the experimental peak shifting to lower frequencies than the half-wave prediction. This behavior indicates a transition away from the resonance-dominated regime implicitly assumed by the

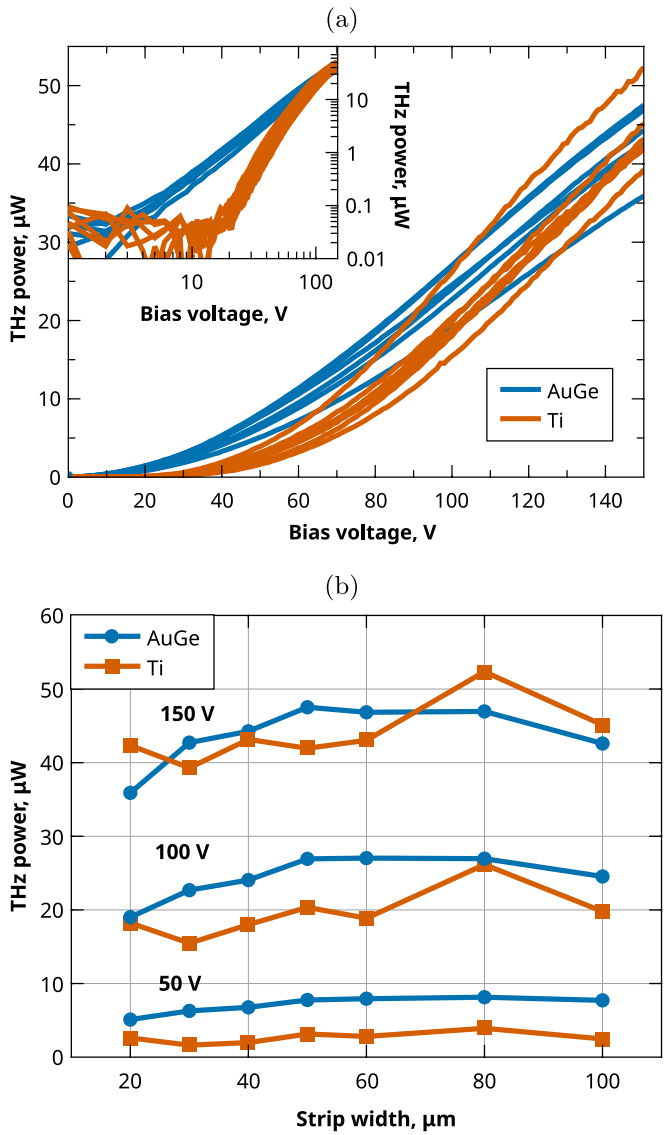

Figure 2. (a) Emitted THz power as a function of bias voltage for all investigated strip widths. The inset shows the same data on a log–log scale. (b) Emitted power as a function of strip width.

dipole expression, toward a regime in which the observed spectral maximum is limited by the bandwidth of the photocarrier-driven feed region and the frequency response of the contact–antenna structure. In particular, when the gap dimension is no longer negligible compared to the antenna length, the feed introduces additional reactive loading in the form of effective capacitance and distributed impedance, causing the PCA to behave as a geometry-dependent low-pass system.

From an impedance perspective, the photoconductive antenna cannot be described as purely inductive or purely capacitive. Instead, its frequency response arises from the combined contributions of the inductive antenna arms, the capacitive photoconductive gap and feed region, and the frequency-dependent surface impedance of the metallic contacts. For wide striplines, the antenna response is dominated by the inductive behavior of the antenna arms, and the capacitive contribution of the gap acts only as a weak perturbation, resulting in a resonance-dominated regime that is well described by classical half-wave dipole theory. As the stripline width is reduced, the relative influence of the gap and feed region on the antenna response increases. The combined effect is a transition to a bandwidth-limited regime in which reactive loading and metal-dependent losses shape the observed frequency response.

In this bandwidth-limited regime, the combined reactive loading and finite conductivity of the metallic contacts act as a frequency-dependent filtering mechanism that progressively suppresses high-frequency components of the generated current and radiated field. As a result, the measured spectral peak is shifted below the simple half-wave estimate and the response broadens, as quantified by the FWHM.

In addition to the strong geometric dependence, a systematic offset between the two metallizations is observed. For strip widths wider than approximately 60 μm, the spectral peak frequency coincides for both

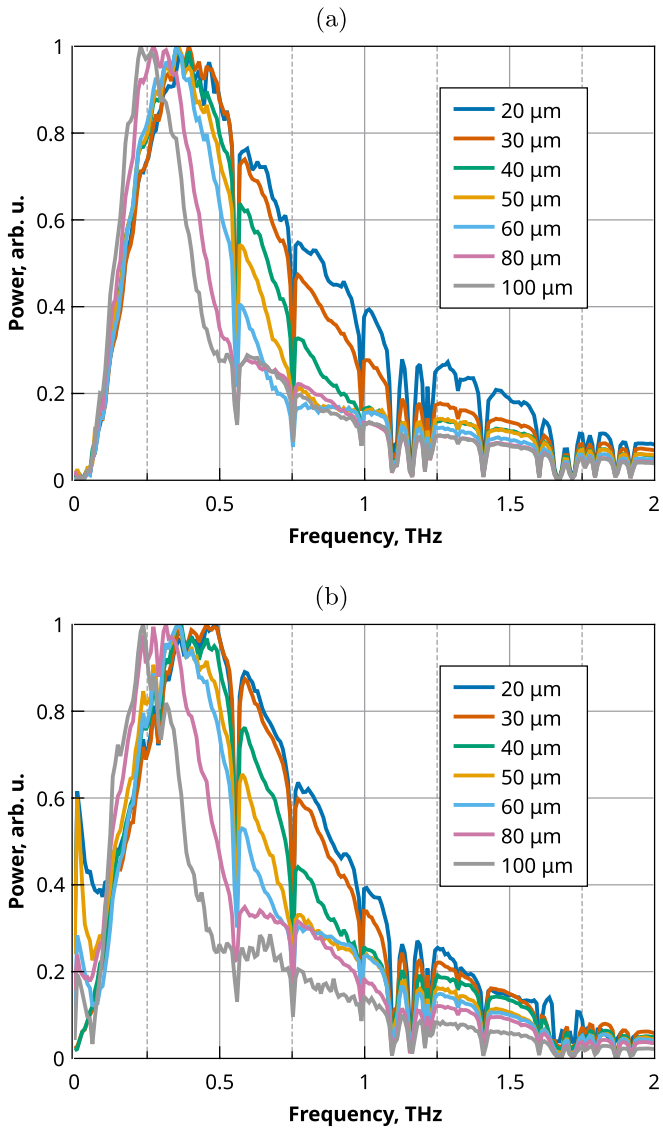

Figure 3. (a) THz-TDS spectra of emitter-detector pairs at various strip widths: (a) AuGe metallization, (b) Ti metallization.

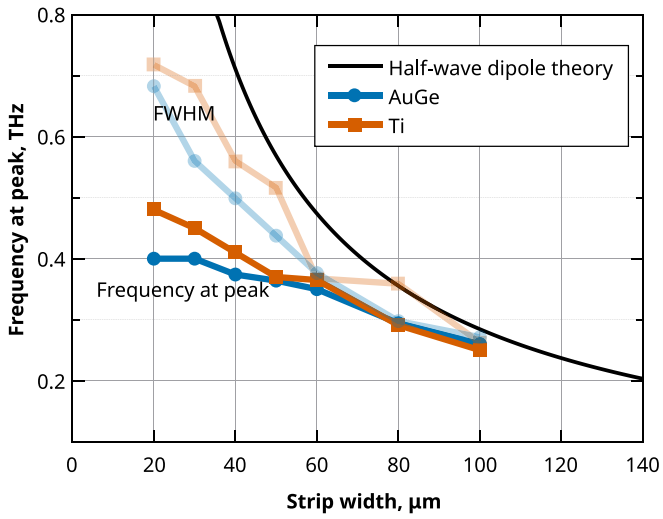

Figure 4. Extracted spectral peaks and bandwidths (FWHM) compared with predictions from classical half-wave dipole theory.

AuGe and Ti devices. This agreement is expected, as the two antenna structures are geometrically identical, the chosen metallization thicknesses are sufficiently large compared to the terahertz skin depth over the relevant band, and the resulting frequency-dependent surface impedance (including inductive reactance) does not differ strongly enough to substantially modify the current distribution in this regime. Consequently, the current distributions along the antenna arms are expected to be comparable, and the PCA response remains predominantly geometry-limited.

As the strip width is reduced, however, the Ti-based antennas consistently exhibit a higher peak frequency together with a broader spectral response compared to AuGe. This behavior indicates a transition to a loss and bandwidth-limited regime in which the metallization increasingly influences the antenna transfer function. In particular, the higher resistive losses of Ti lead to a faster decay of antenna currents and stored electromagnetic energy, corresponding to a shorter energy-decay time τ_{ant}. This enhanced damping suppresses long-lived, low-frequency current components more strongly, reweighting the emitted spectrum toward higher frequencies and broadening the response. Importantly, this shift does not imply a higher intrinsic resonance frequency of the Ti antennas, but rather reflects a metal-dependent filtering of the broadband photocarrier excitation by the contact–antenna structure.

Within this framework, shifting the spectral peak of short-dipole PCAs toward higher frequencies is expected to require mitigation of the reactive loading and bandwidth limitations imposed by the contact–antenna structure. Capacitive loading may, in principle, be reduced by enlarging the electrode gap or by introducing air trenches in the dielectric using approaches such as deep reactive ion etching [22] or laser interference ablation [23]. At terahertz frequencies, the finite skin depth and surface impedance of metallic contacts can render the antenna current distribution sensitive to nanoscale surface morphology. Controlled surface corrugation oriented perpendicular to the current flow may increase the effective surface impedance through enhanced current crowding and scattering, potentially leading to faster antenna current decay and a suppression of long-lived, low-frequency components. In a strongly damped regime, such mechanisms could reweight the emitted spectrum toward higher frequencies, thereby influencing both the high-frequency roll-off and the observed spectral peak position.

4. Conclusions

We have experimentally investigated terahertz photoconductive antennas based on coplanar striplines on GaAs, focusing on the influence of stripline width and contact metallization on emitted terahertz power and spectral response. AuGe/Ni/Au contacts provide higher emission efficiency at low bias due to favorable carrier injection, whereas Ti-based devices, initially limited by Schottky barriers, achieve comparable output at high bias fields. Terahertz time-domain spectroscopy confirms that reducing the stripline width shifts the spectral maximum toward higher frequencies, and for sufficiently wide striplines the observed response is reasonably described by classical half-wave dipole theory.

For narrower striplines, systematic deviations from the dipole model are observed, indicating a transition to a bandwidth-limited regime governed by the combined response of the photocarrier feed region and the contact–antenna structure. In this regime, Ti-based antennas exhibit higher spectral peak frequencies and broader bandwidths than AuGe-based devices, consistent with increased resistive losses and surface impedance that are associated with faster antenna current decay and suppression of low-frequency components. These results demonstrate that, at higher terahertz frequencies, the performance of photoconductive antennas is increasingly constrained by the finite, frequency-dependent impedance of metallic contacts, emphasizing the importance of contact and geometry engineering for next-generation PCAs aimed at spectral maxima shifted toward higher frequencies.

Acknowledgments

The authors gratefully acknowledge Ričardas Norkus and Andrzej Urbanowicz for their assistance with the experimental setups and for valuable discussions. This project was funded by the Research Council of Lithuania (LMTLT), agreement No S-TPP-23-11.

Data availability statement

All data that support the findings of this study are included within the article (and any supplementary files).

References

[1] Bacon D R, Madéo J and Dani K M 2021 *J. Opt.* **23** 064001
[2] Burford N M and El-Shenawee M O 2017 *Opt. Eng., Bellingham* **56** 010901
[3] Isgandarov E, Ropagnol X, Singh M and Ozaki T 2021 *Frontiers of Optoelectronics* **14** 64–93
[4] Berry C W and Jarrahi M 2012 *Journal of Infrared, Millimeter, and Terahertz Waves* **33** 1182–9
[5] Tani M, Matsuura S, Sakai K and Nakashima S I 1997 *Appl. Opt.* **36** 7853–9
[6] Cai Y, Brener I, Lopata J, Wynn J, Pfeiffer L and Federici J 1997 *Appl. Phys. Lett.* **71** 2076–8
[7] Nguyen T K, Kim W T, Kang B J, Bark H S, Kim K, Lee J, Park I, Jeon T I and Rotermund F 2017 *Opt. Commun.* **383** 50–6
[8] Alfihed S, Foulds I G and Holzman J F 2021 *Sensors* **21** 3131
[9] Shi X, Wang K, Gu J, An Y, Jia R, Tian Z, Ouyang C, Han J and Zhang W 2021 *Advanced Photonics Research* **2** 2000036
[10] Jepsen P U, Jacobsen R H and Keiding S R 1996 *Journal of the Optical Society of America B* **13** 2424–36
[11] Miyamaru F, Saito Y, Yamamoto K, Furuya T, Nishizawa S and Tani M 2010 *Appl. Phys. Lett.* **96** 211104
[12] Shi W, Hou L and Wang X 2011 *J. Appl. Phys.* **110** 023111
[13] Nevinskas I, Kamarauskas M, Geižutis A, Kovalevskij V, Bičiūnas A, Urbanowicz A, Norkus R and Ikamas K 2024 *Lith. J. Phys.* **64** 253–8
[14] Shi W, Hou L, Liu Z and Tongue T 2009 *Journal of the Optical Society of America B* **26** A107–12
[15] Ghita R V, Logofatu C, Negrila C, Manea A S, Cernea M and Lazarescu M F 2005 *J. Optoelectron. Adv. Mater.* **7** 3033–7 (https://old.joam.inoe.ro/arhiva/pdf7_6/Ghita.pdf)
[16] Vieweg N, Mikulics M, Scheller M, Ezdi K, Wilk R, Hübers H and Koch M 2008 *Opt. Express* **16** 19695
[17] Hou L, Shi W, Han X and Yan Z 2012 *Electron. Lett.* **48** 780–1
[18] Lambsdorff M, Kuhl J, Rosenzweig J, Axmann A and Schneider J 1991 *Appl. Phys. Lett.* **58** 1881–3
[19] Sun C and Zhang A 2019 Ion-beam modified terahertz GaAs photoconductive antenna *Advances in Photodetectors - Research and Applications* ed K Chee (IntechOpen) chap 3 (https://doi.org/10.5772/intechopen.79693)
[20] Sze S and Ng K K 2006 *Physics of Semiconductor Devices* 1st ed (Wiley) (https://doi.org/10.1002/0470068329)
[21] Ridley B K 1989 *Semicond. Sci. Technol.* **4** 1142
[22] Byun I and Kim J 2010 *J. Micromech. Microeng.* **20** 055024
[23] Müller D W, Fox T, Grützmacher P G, Suarez S and Mücklich F 2020 *Sci. Rep.* **10** 3647